J. Fluid Mech. (2005), *vol.* 530, *pp.* 369–378.
doi:10.1017/S0022112005003770 Printed in the United Kingdom

Injection and coalescence of bubbles in a very viscous liquid

By F. J. HIGUERA

E. T. S. Ingenieros Aeronáuticos, Pza. Cardenal Cisneros 3, 28040 Madrid, Spain

(Received 1 September 2004 and in revised form 31 January 2005)

The periodic generation of bubbles by injection of a gas at constant flow rate through an orifice at the bottom of a quiescent liquid of high viscosity is investigated numerically. The volume of the bubbles is determined as a function of a capillary number and a Bond number in the absence of inertial effects. Pairs of bubbles coalesce in the vicinity of the orifice when the capillary number is higher than a critical value that depends on the Bond number, but the final volume of the bubbles still follows a well-known scaling law at large capillary numbers. Qualitative experimental visualizations are presented that display the sequences of detachment and coalescence computed numerically.

1. Introduction

Most of the extensive research carried out on the generation of bubbles by injection of gas into a liquid at rest has been devoted to the important case of liquids of small viscosity, for which the flow induced by the expansion and rise of the bubbles is dominated by inertial effects; see Kumar & Kuloor (1970), Clift, Grace & Weber (1978), Räbiger & Vogelpohl (1986) and Sadhal, Ayyaswamy & Chung (1997) for reviews. Applications include direct-contact operations in chemical, metallurgical, and biomedical systems, among many others. The opposite case of bubble generation in very viscous liquids is of interest in connection with polymer melts (Bird, Armstrong & Hassager 1987) and molten glasses and magmas (Sahagian 1985; Manga & Stone 1994), for example, but it has been comparatively less studied. Using a balance of buoyancy and viscous forces on the surface of each bubble, Davidson & Schuler (1960) proposed that the volume of the bubbles injected in a very viscous quiescent liquid increases as the 3/4 power of the gas flow rate and is independent of the radius of the injection orifice. This estimate is intended to apply for high gas flow rates, for which the effect of the surface tension acting across the contact line of the attached bubble with the solid surface of the orifice is negligible. At very small flow rates, on the other hand, viscous forces are negligible during most of the growth of the bubble, whose shape is determined by a hydrostatic balance of buoyancy and surface tension. Longuet-Higgins, Kerman & Lunde (1991) computed the equilibrium shapes of attached bubbles and the volume at which equilibrium ceases to be possible and the bubble should detach. In orders of magnitude, the volume of the bubble at detachment, V, is given in this small-flow-rate regime by the hydrostatic balance $\rho g V \sim \sigma a$, or $V/a^3 \sim 1/B$ in dimensionless terms. Here ρ is the density of the liquid, σ is the liquid–gas surface tension, a is the radius of the injection orifice, g is the acceleration due to gravity, and

$$B = \frac{\rho g a^2}{\sigma} \tag{1.1}$$

is a Bond number. If the growth of the bubble is due to the injection of a gas at flow rate Q, then the velocity induced in the liquid by the expansion of the bubble is $v = O(Q/V^{2/3})$ and the viscous force of the liquid on the surface of the bubble is $F_v = O[(\mu v/V^{1/3})V^{2/3}] = O(\mu Q/V^{1/3})$, where μ is the viscosity of the liquid. This force becomes of the order of the buoyancy force ($F_v \sim \rho g V \sim \sigma a$) when $Q \sim \rho g V^{4/3}/\mu$ or, using the estimate of V above, when $Ca \sim 1/B^{1/3}$, where

$$Ca = \frac{\mu Q}{\sigma a^2} \tag{1.2}$$

is a capillary number. At higher flow rates, the surface tension becomes negligible in the balance of forces on the bubble, which reduces to $F_v \sim \rho g V$, leading to (Davidson & Schuler 1960)

$$\frac{V}{a^3} \sim \left(\frac{Ca}{B}\right)^{3/4}. \tag{1.3}$$

The hydrostatic regime thus corresponds to $Ca \ll 1/B^{1/3}$, and the Davidson & Schuler high-flow-rate regime should be attained for $Ca \gg 1/B^{1/3}$. Wong, Rumschitzki & Maldarelli (1998) numerically computed the time evolution of a single bubble from onset to detachment for a variety of Bond and capillary numbers, describing the transition between hydrostatic and high-flow-rate regimes. Zhang & Stone (1997) extended this analysis to take into account the viscosity of the injected fluid.

An additional complexity arises, however. The ratio of the growth time of a bubble, $t_{growth} \sim V/Q$, to the time it takes for a detached bubble to rise a distance of the order of its size, $t_{rise} \sim V^{1/3}/U$, with the rise velocity U estimated from the balance of buoyancy and viscous drag $\rho g V \sim \mu U V^{1/3}$, is $t_{growth}/t_{rise} \sim (V^{4/3}/a^4)B/Ca$. This ratio is large in the hydrostatic regime but becomes of order unity in the transition regime and beyond, leading to interaction between successive bubbles and the possibility of coalescence in the vicinity of the injection orifice. The present work is devoted to describing these multi-bubble processes at moderately large capillary numbers, at which the flow is time periodic.

2. Formulation

Consider the simplest case of a constant flow rate of an incompressible gas of negligible density and viscosity injected through a single circular orifice at the horizontal bottom of the liquid. Let $f_i(\boldsymbol{x}, t) = 0$ denote the surface of the ith bubble, with $f_i > 0$ in the liquid. In the absence of inertia ($\rho Q/\mu a \ll 1$), the flow induced in the liquid by the bubble growing at the orifice ($i = 0$) and the bubbles detached previously ($i = 1, 2, \ldots$) satisfies the Stokes equations

$$\nabla \cdot \boldsymbol{v} = 0, \qquad 0 = -\nabla p - B\boldsymbol{i} + \nabla^2 \boldsymbol{v} \tag{2.1}$$

with the boundary conditions

$$\frac{\mathrm{D}f_i}{\mathrm{D}t} = 0, \qquad -p\boldsymbol{n}_i + \tau' \cdot \boldsymbol{n}_i = (\nabla \cdot \boldsymbol{n}_i - p_{g_i})\boldsymbol{n}_i \tag{2.2a, b}$$

at the surfaces of the bubbles, and the condition $\boldsymbol{v} = 0$ at the solid bottom ($x = 0$) and at infinity, where $p + Bx$ is a constant. Here distances and times are scaled with the radius of the orifice a and the viscous time $\mu a/\sigma$; $\boldsymbol{i}$ is a unit vector pointing upward; $\mathrm{D}/\mathrm{D}t = \partial/\partial t + \boldsymbol{v} \cdot \nabla$ is the material derivative at points of the bubble surfaces; $\boldsymbol{n}_i = \nabla f_i/|\nabla f_i|$; τ' is the viscous stress tensor, given by the Navier–Poisson law; and p_{g_i} is the dimensionless pressure of the gas in the ith bubble. These pressures are determined by the conditions that the volumes of the detached bubbles ($i = 1, 2, \ldots$)

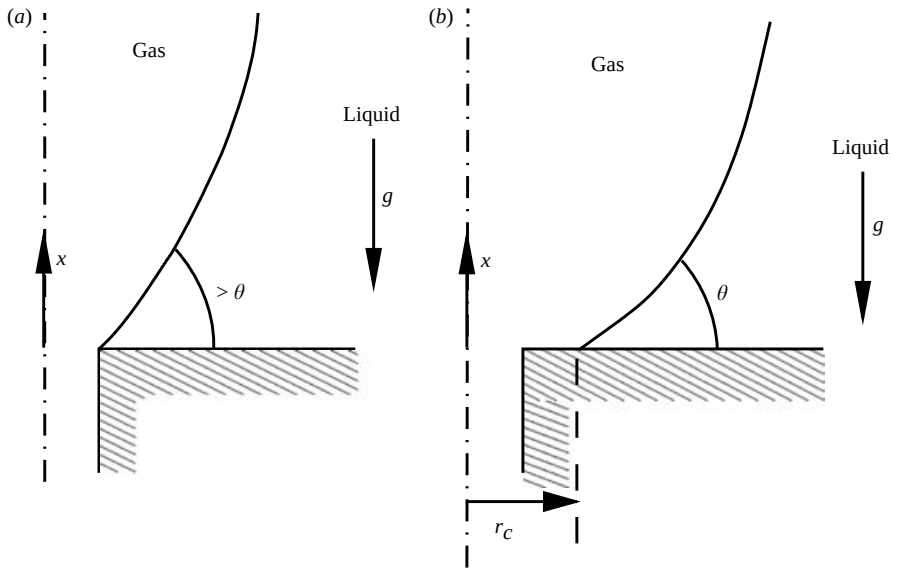

FIGURE 1. Detail of the contact line.

do not change with time and the dimensionless volume V_0 of the growing bubble ($i = 0$) increases as $\mathrm{d}V_0/\mathrm{d}t = Ca$. An additional condition is needed at the contact line of the growing bubble with the solid. Here the contact line will be taken to coincide with the edge of the orifice when the angle of the liquid–gas surface with the horizontal bottom is larger than the contact angle (i.e. when $-n_{x_0} < \cos\theta$, where n_{x_0} is the vertical component of the unit normal $\boldsymbol{n}_0$ to the attached bubble), and to spread away from the orifice, with the liquid–gas surface making a constant contact angle with the solid bottom ($-n_{x_0} = \cos\theta$) otherwise; see figure 1. The contact angle θ is a third parameter of the problem, along with the Bond and capillary numbers defined in (1.1) and (1.2).

Time-periodic axisymmetric solutions have been computed using a standard boundary element method to solve the Stokes equations (Pozrikidis 1992) and a second-order Runge–Kutta method to advance the material nodes at the surfaces according to (2.2*a*). The implementation follows that of Wong *et al.* (1998) and Pozrikidis (2002). The number of nodes used to discretize each surface ranges from 60 to 120 in typical computations, depending on the length of the meridional section of the surface.

To keep the computations affordable, the number of bubbles simultaneously followed is limited to three by removing the uppermost bubble when a new bubble begins to grow at the orifice. This approximation brings in a loss of accuracy because the velocity induced by a single rising bubble decreases only as the inverse of the distance to the bubble, making long-range interactions between bubbles important in viscosity-dominated flows (Manga & Stone 1993, 1995). Numerical tests in which one more bubble is kept show that the effect of the extra bubble on the growth of the bubble attached to the orifice is small, and its influence on the coalescence process (to be discussed below) is only moderate. This may be due to the combination of the restraining influence of the solid bottom, which reduces the velocities induced by the far bubbles, and the effect of the expansion of the bubble growing at the orifice, which dominates the local flow and renders long-range interactions less important than they are between separated bubbles far from the orifice. Thus, the velocity induced by a bubble of volume V rising at a speed U at a distance H above the bottom on a

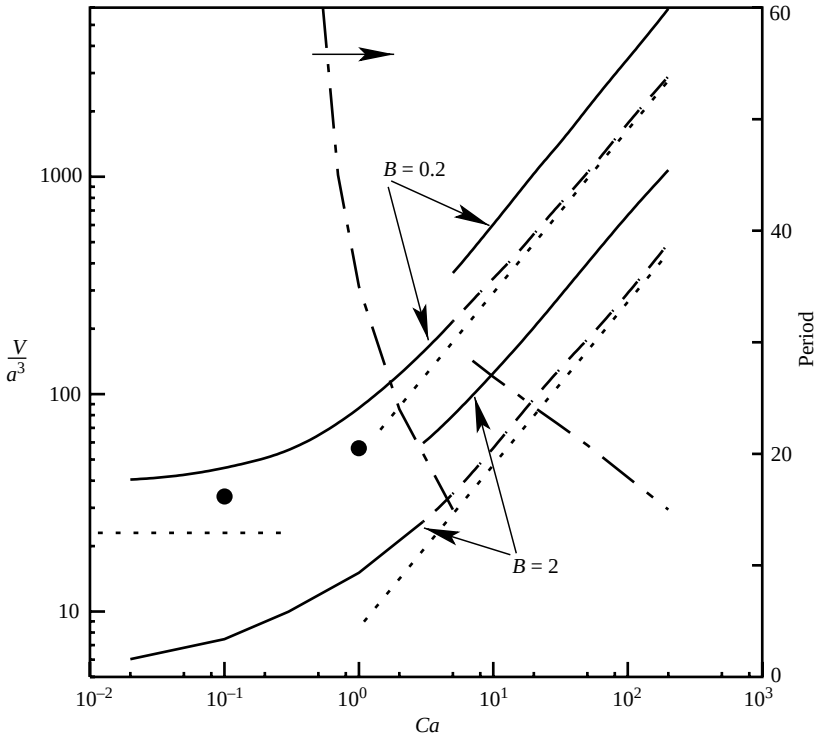

FIGURE 2. The two pairs of solid curves give the computed dimensionless volume of the bubbles as a function of the capillary number, below and above the critical capillary number at which coalescence begins, for two values of the Bond number. The dashed curves give the volume of the first bubble of each couple before undergoing coalescence. The dotted lines at the right have slope 3/4. The horizontal dotted line at the left gives the volume of the bubbles in the quasi-hydrostatic regime, according to Longuet-Higgins *et al.* (1991). The two black circles are volumes computed by Wong *et al.* (1998) for $B = 0.2$. The dash-and-dot curve gives the period of the bubble generation process as a function of the capillary number for $B = 0.2$.

bubble of similar volume attached to the injection orifice is of order $U(V^{1/3}/H)^2$. The ratio of this velocity to the $O(Q/V^{2/3})$ velocity due to the growth of the attached bubble is of order $(V^{1/3}/H)^2$, where use has been made of (1.3) and the estimate of U in the previous section. The influence of the nth bubble above the bottom should therefore decrease as $1/n^2$ in the high-flow-rate regime.

An additional criterion is needed to handle the surface reconnections that occur at the detachment of a growing bubble and at the coalescence of two bubbles. Here a reconnection will be assumed to occur when the distance between the two approaching surfaces becomes smaller than a certain cutoff of the order of the separation between the material nodes. Smoothing after reconnection is taken care of by cubic splines, used also for interpolation purposes in the rest of the computation. The results obtained by this procedure are not very sensitive to the precise value of the cutoff, which has been varied from the length of the meridional section divided by the number of nodes to zero (by letting the surfaces intersect).

3. Results and discussion

Figure 2 shows the dimensionless volume of the bubbles as a function of the capillary number (dimensionless flow rate) for two values of the Bond number and

$\theta = 45°$. In each case, the volume tends to a finite value in the hydrostatic limit $Ca \to 0$. Longuet-Higgins *et al.* (1991) approximated this limiting volume by the volume of the limiting equilibrium shape above its neck (when a neck exists); the corresponding value for $B = 0.2$ is given by the dotted horizontal line at the left-hand side of figure 2. The volumes computed for small values of Ca are above this line, probably due to the increase and redistribution of the bubble volume during the last, non-hydrostatic stage of growth in the presence of a solid wall. The numerical results show that the region around the neck experiences fast changes in this stage, but the shrinking of the neck is fairly slow, which delays the terminal pinchoff. The slow pinching of the neck seems to follow the non-universal, quadratic breakup dynamics uncovered by Doshi *et al.* (2003) and further investigated by Suryo, Doshi & Basaran (2004) when a bubble of zero viscosity breaks in a high-viscosity liquid (see figure 3*e*, *f* below). The pinching here does not tend to the terminal self-similar regime studied by Sierou & Lister (2003) for cases when the bubble has a finite viscosity. For comparison, the two black circles of figure 2 correspond to volumes computed by Wong *et al.* (1998) for a single bubble detaching from the tip of a vertical tube. These authors assume that the radius of the neck decreases as the square root of the time to pinchoff during the final stages of the process.

The results for large values of the capillary number tends to the 3/4 power law (1.3) both for single-bubble computations (dashed curves of figure 2) and when coalescence is taken into account (solid curves), although the proportionality factor to be inserted in (1.3) is different in each case. Moreover, the high-Ca asymptotes for the two values of B displayed in figure 2 practically coincide when the dimensionless volume is plotted versus Ca/B, in accordance with the scaling of Davidson & Schuler (1960).

The following discussion refers to the case of $B = 0.2$. Results for other values of the Bond number are similar. The minimum capillary number at which coalescence occurs is a little below $Ca = 5$. Contrarily to what is often reported for bubbles injected in liquids of low viscosity (see e.g. the experimental results of Zhang & Shoji 2001), here coalescence occurs for the first time between bubbles that have already detached from the orifice. For $Ca = 5$, bubbles coalesce at a height of about 30 radii above the injection orifice. This value is obtained by extrapolating the paths of two successive bubbles that approach each other rather than by direct computation, which is made cumbersome by the need to follow many bubbles in the space between the orifice and the location of coalescence. The minimum Ca for coalescence is thus sensitive to the long-range interactions discussed above, and the computed value is probably not very accurate.

The height of coalescence decreases when the capillary number increases. The leading bubble of each couple is almost round while it grows, and becomes an oblate spheroid with a slightly concave base upon detachment. The trailing bubble grows in the presence of the leading bubble and is more elongated than it (see figures 3 and 4). The oblate (prolate) shape of the leading (trailing) bubble of an axisymmetrically interacting pair has been observed and explained by Manga & Stone (1993) in terms of the flow-induced interaction between the bubbles of the pair (see their figure 4). Thus, the upward flow induced by the leading bubble, idealized as an upward point force, has convergent streamlines at the position of the trailing bubble, which is therefore strained vertically. The analogous flow induced by the trailing bubble has divergent streamlines at the position of the leading bubble, which is strained radially in a horizontal plane. The large bubble that results when a round and an elongated bubble coalesce rises faster that the component bubbles, and its effect on the growth of the following bubble at the orifice rapidly decreases. At $Ca = 7$ the coalescence of two

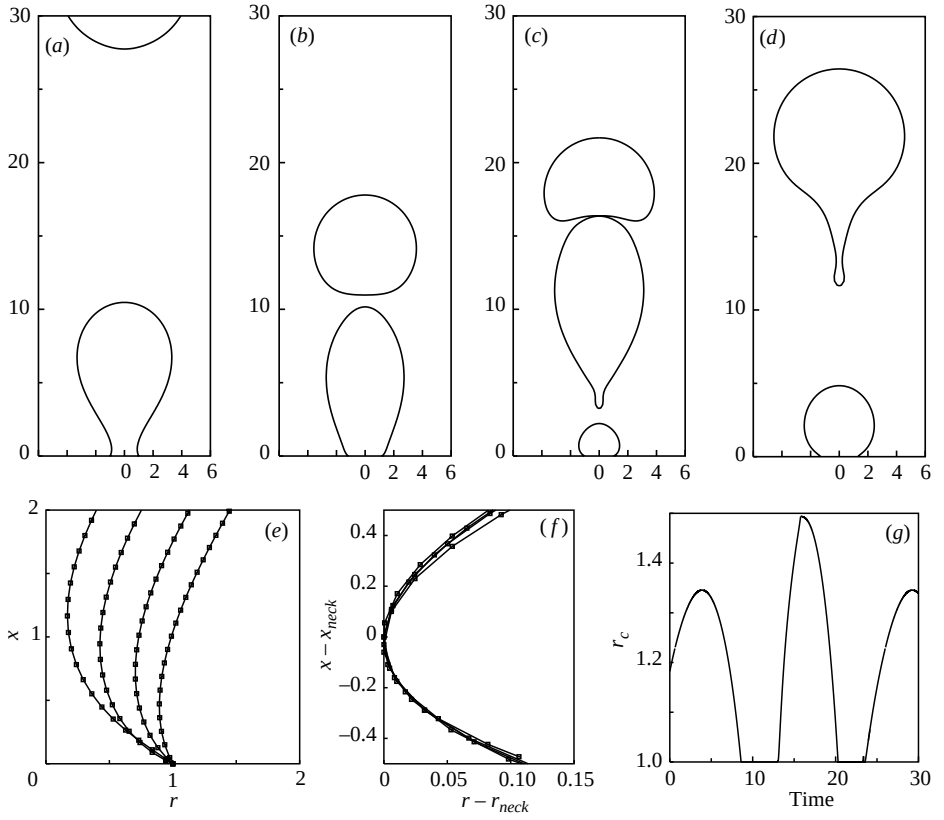

FIGURE 3. Four snapshots of the detachment and coalescence of two bubbles for $Ca = 15$ and $B = 0.2$. The first bubble detaches between (*a*) and (*b*); the second bubble detaches between (*b*) and (*c*); coalescence occurs immediately after (*c*); and a secondary bubble is about to be shed in (*d*). The time elapsed from the detachment of the previous bubble (visible in the upper part of (*a*)) is 11.55 (*a*), 21.15 (*b*), 25.95 (*c*), and 29.55 (*d*). The period of the process is 25.37. (*e*) A region around the neck of the attached bubble in (*a*) at four instants in time as the detachment of the bubble is approached (11.55, 12.30, 13.05 and 13.65; detachment occurs at about 14). The squares are the computational nodes. (*f*) A further close-up of this region with the profiles shifted to take the neck ($x_{neck}(t)$, $r_{neck}(t)$) to the origin. The near collapse of the shifted profiles shows the agreement with the local dynamics reported by Doshi *et al.* (2003) and Suryo *et al.* (2004) during these stages of the neck formation. (*g*) The displacement of the contact line on the horizontal bottom during a period of the process.

bubbles occurs at about the same time as the detachment of the leading bubble of the following couple. Above $Ca \approx 7$ the retraction of the lower surface of the bubble after coalescence is accompanied by the shedding of a small bubble, which is left behind by the main rising bubble (as in figures 3*d* and 4*d*; see also Manga & Stone 1993). This secondary bubble has very little effect on the flow and is artificially suppressed in the computations. Test computations in which the small bubble is retained have shown that it is captured and absorbed by the following bubble without any noticeable influence on its evolution.

When the capillary number increases above $Ca \approx 15$, coalescence occurs before the trailing bubble of each couple has had time to detach from the orifice, so that the sequence detachment–detachment–coalescence described above and illustrated in figure 3 changes to the sequence detachment–coalescence–detachment illustrated in

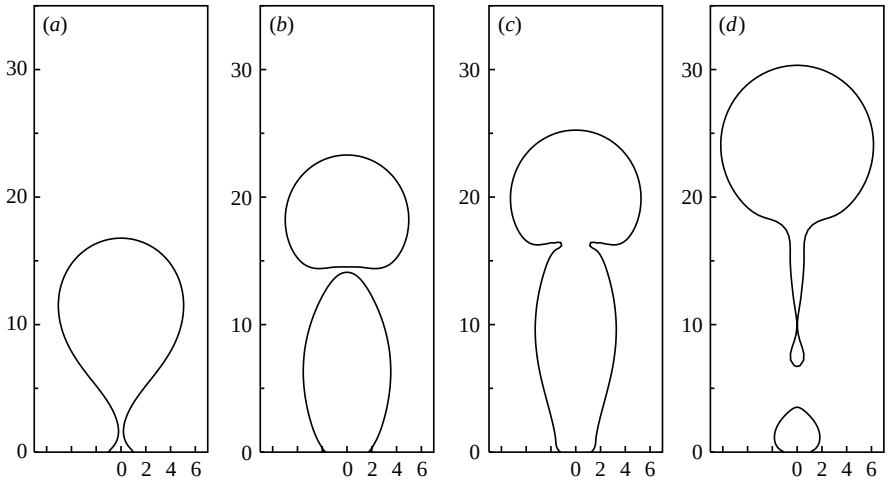

FIGURE 4. Four snapshots of the detachment and coalescence of two bubbles for $Ca = 50$ and $B = 0.2$. The first bubble detaches between (*a*) and (*b*); coalescence occurs between (*b*) and (*c*), when the second bubble is still attached to the orifice; the second bubble detaches between (*c*) and (*d*). The time elapsed from the detachment of the previous bubble (not visible in the figure) is 11.17 (*a*), 15.97 (*b*), 17.17 (*c*), and 19.27 (*d*). The period of the process is 18.91.

figure 4. Here, and in part of the evolution displayed in figure 3, the mechanism of bubble deformation described by Manga & Stone is reinforced by the flow induced by the growth of the trailing bubble. If the growth of this bubble is idealized as a point source flow, it is clear that it will help to strain the leading bubble horizontally. On the other hand, the leading bubble offers less viscous resistance to deformation than the liquid that would occupy its volume if it were not present, and thus the leading bubble favours the vertical elongation of the attached bubble over its horizontal radial expansion. The detachment of the compound bubble (which in some cases resembles the plumes observed by Whitehead & Luther 1975) occurs soon after coalescence, and it is followed by the shedding of one or a few small secondary bubbles from its retracting lower surface (figure 4*d*). The rapid succession of coalescence and detachment of the compound bubble remains when the capillary number is increased. The change in the bubble formation sequence is not marked by any noticeable change of the final volume of the bubble as a function of the capillary number. The value of the capillary number at which the sequence changes is slightly affected by the artificial suppression of old separated bubbles discussed in the previous section. Tests carried out on suppressing one more bubble that does not participate in the coalescence (like the upper bubble still visible in figure 3*a*) show that this slightly decreases the capillary number at which the sequence changes, in line with the results of Manga & Stone (1993, 1995).

The formation sequence reverts to detachment–detachment–coalescence for capillary numbers higher than about 100. Then the detachment of the leading bubble of each couple is followed by the shedding of a small secondary bubble, which effectively increases the rate of retraction of the lower surface of the leading bubble and the gap between its base and the top of the following bubble growing at the orifice. The effect is to postpone coalescence until the tailing bubble has detached from the orifice.

Coalescence of three or more bubbles in the vicinity of the orifice, which is a well-known feature of bubble generation in liquids of low viscosity (Zhang & Shoji

2001; see also Tritton & Egdell 1993), has not been observed in these computations even at the highest capillary number that have been attained, about $Ca = 200$.

Numerical results for other values of the Bond number are similar to the results discussed above. Both the dimensionless volume of the bubbles at a given capillary number and the minimum capillary number at which coalescence occurs decrease with increasing the Bond number. At $B = 2$, coalescence begins when $Ca \approx 3$ (figure 2), and the two coalescing bubbles have detached from the orifice for all the capillary numbers that have been computed; the sequence detachment–coalescence–detachment has not been observed at $B = 2$. On the other hand, this sequence occurs in the range $200 \leqslant Ca \leqslant 300$, approximately, when $B = 0.03$.

The numerical results have been compared with visualizations of bubble formation and coalescence in silicone oil (Dow-Corning 200, 10000 cSt), with properties $\mu = 9.68\,\mathrm{s\,Pa}$ (at 25°C), $\rho = 968\,\mathrm{Kg\,m^{-3}}$, $\sigma = 2.15 \times 10^{-2}\,\mathrm{N\,m^{-1}}$. Air was injected through a vertical hypodermic needle of internal diameter $2a = 0.25\,\mathrm{mm}$ to $0.5\,\mathrm{mm}$ (25G to 21G) sticking out of the centre of the base of a vertical cylindrical container of 8.6 cm diameter filled with oil to a height of 20 cm above the tip of the needle. The pressure drop in the needle and the feeding line was used to minimize the variations of the air flow rate, which was roughly estimated from the volumes of video recorded bubbles (assumed axisymmetric). The purpose of these experiments is to show that the sequences of detachment and coalescence predicted numerically occur in reality, but no attempt has been made to reproduce the conditions of the computations or to accurately control and measure the flow rate. Figure 5 shows sample photographs, digitized contours, and contours computed numerically for values of the non-dimensional parameters B and Ca similar to those of the experiments. The small bubbles that appear in the photographs are shed by the larger bubbles as explained before. These small bubbles rise very slowly and therefore accumulate when air has been continuously injected for some time, but they do not seem to affect the evolution of the large bubbles much. Figure 5(a) shows the coalescence of a separated bubble and a bubble still attached to the injection needle. Numerical results for the values of B and Ca of the experiment but with the bubbles growing at an orifice in a horizontal wall show that the trailing bubble detaches before coalescing with the bubble above it. This discrepancy may be due to the influence of the solid boundary or to the inaccurate determination of the flow rate in the experiment. The rightmost contour in figure 5(a) is a numerical result for $B = 0.03$ and a capillary number smaller than the value estimated for the experiment. The four photographs of figure 5(b) capture the detachment of a bubble followed by its coalescence with the bubble above it, while figure 5(c) shows that this sequence of detachment–detachment–coalescence also occurs at larger capillary numbers.

4. Conclusions

The axisymmetric time-periodic creeping flow induced in a very viscous liquid by the injection of a constant gas flow rate through a horizontal submerged orifice has been computed. The results are expressed in terms of three dimensionless parameters: a capillary number, a Bond number, and the contact angle of the liquid with the solid bottom. The transition from quasi-static generation of independent bubbles at low capillary numbers to the viscosity- and buoyancy-controlled regime of Davidson & Schuler (1960) at very high capillary numbers has been described. Coalescence of bubbles in pairs has been shown to occur in two possible ways in the vicinity of the orifice when the capillary number increases above a certain critical value that depends

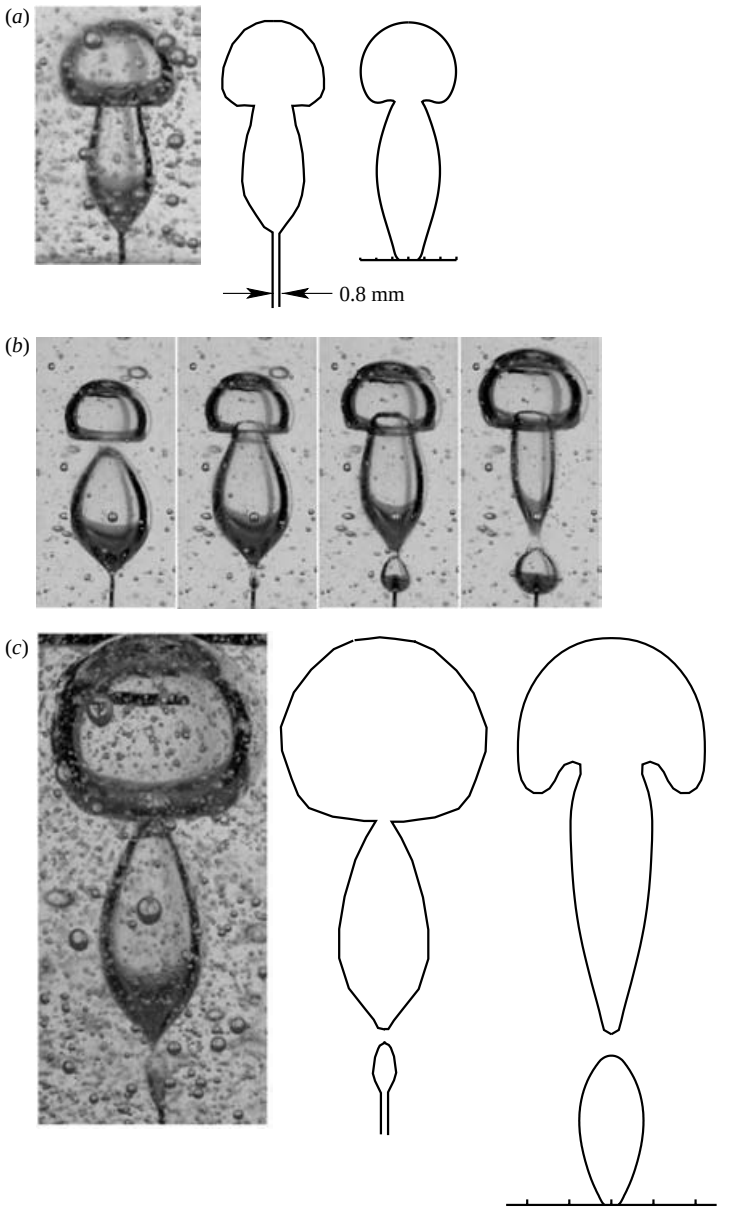

FIGURE 5. Sample experimental results. The outer diameter of the needle is 0.8 mm in all cases, which gives the scale of each row of the figure. The inner diameter is 0.5 mm ($B = 0.03$). In (*a*), for $Q \sim 0.95\,\mathrm{cm}^3\,\mathrm{s}^{-1}$ ($Ca \sim 700$), coalescence has just occurred between a separated bubble and an attached bubble. Shown are a raw photo, the contour of the bubble extracted from the photo, and a contour computed at a time shortly after coalescence for $B = 0.03$ and $Ca = 300$ but with the gas flowing from an orifice in a horizontal wall. In (*b*), for $Q \sim 1.3\,\mathrm{cm}^3\,\mathrm{s}^{-1}$ ($Ca \sim 950$), the sequence has changed to detachment–detachment–coalescence. This sequence is maintained in (*c*), for $Q \sim 20\,\mathrm{cm}^3\,\mathrm{s}^{-1}$ ($Ca \sim 15000$). The rightmost contour in (*c*) is a numerical result for the same values of B and Ca as the experiment. The values quoted for the flow rate are coarse estimations for which no accuracy is claimed. A Reynolds number representative of the flow is $Re = (\rho Q/\mu a)(B/Ca)^{1/4}$, where the second factor is a measure of $a/V^{1/3}$ (see (1.3)). Values of this Reynolds number for the three cases displayed are 3.1×10^{-2}, 3.9×10^{-2} and 0.3, respectively.

on the Bond number. The volume of the resulting bubbles is larger than predicted by single-bubble computations, but it still increases as $Ca^{3/4}$ at the highest capillary numbers for which time-periodic solutions have been computed. The numerical results are in qualitative agreement with visualizations of bubble coalescence upon injection of air in a silicone oil.

The author is grateful to the referees for their comments, which have greatly improved the paper. This work was supported by the Spanish Ministerio de Ciencia y Tecnología project DPI2002–4550–C07-5.

REFERENCES

Bird, R. B., Armstrong, R. C. & Hassager, U. 1987 *Dynamics of Polymeric Liquids*. Wiley.

Clift, R., Grace, J. R. & Weber, M. E. 1978 *Bubbles, Drops, and Particles*. Academic.

Davidson, J. F. & Schuler, B. O. G. 1960 Bubble formation at an orifice in a viscous liquid. *Trans. Inst. Chem. Engrs* **38**, 144–154.

Doshi, P., Cohen, I., Zhang, W. W., Siegel, M., Howell, P., Basaran, O. A. & Nagel, S. R. 2003 Persistence of memory in drop breakup: the breakdown of universality. *Science* **302**, 1185–1188.

Kumar, R. & Kuloor, N. R. 1970 The formation of bubbles and drops. *Adv. Chem. Engng* **8**, 255–368.

Longuet-Higgins, M. S., Kerman, B. R. & Lunde, K. 1991 The release of air bubbles from an underwater nozzle. *J. Fluid Mech.* **230**, 365–390.

Manga, M. & Stone, H. A. 1993 Buoyancy-driven interactions between two deformable viscous drops. *J. Fluid Mech.* **256**, 647–683.

Manga, M. & Stone, H. A. 1994 Interactions between bubbles in magmas and lavas: Effects of the deformation. *J. Vulcanol. Res.* **63**, 269–281.

Manga, M. & Stone, H. A. 1995 Collective hydrodynamics of deformable drops and bubbles in dilute low Reynolds number suspensions. *J. Fluid Mech.* **300**, 231–263.

Pozrikidis, C. 1992 *Boundary Integral and Singularity Methods for Linearized Viscous Flows*. Cambridge University Press.

Pozrikidis, C. 2002 *A Practical Guide to Boundary Element Methods*. Chapman and Hall/CRC.

Räbiger, N. & Vogelpohl, A. 1986 Bubble formation and its movement in newtonian and non-newtonian liquids. In *Encyclopedia of Fluid Mechanics*, Vol. 3, Chapter 4 (ed. N. P. Cheremisinoff). Gulf.

Sadhal, S. S., Ayyaswamy, P. S. & Chung, J. N. 1997 *Transport Phenomena with Drops and Bubbles*, Chapter 7. Springer.

Sahagian, D. L. 1985 Bubble migration and coalescence during solidification of basaltic lava flows. *J. Geol.* **93**, 205–211.

Sierou, S. & Lister, J. R. 2003 Self-similar solutions for viscous capillary pinch-off. *J. Fluid Mech.* **497**, 381–403.

Suryo, R., Doshi, P. & Basaran, O. 2004 Non-self-similar, linear dynamics during pinch-off of a hollow annular jet. *Phys. Fluids* **16**, 4177–4184.

Tritton, D. J. & Egdell, C. 1993 Chaotic bubbling. *Phys. Fluids* A **5**, 503–505.

Whitehead, J. A. & Luther, D. S. 1975 Dynamics of laboratory diapir and plume models. *J. Geophys. Res.* **10**, 705–717.

Wong, H., Rumschitzki, D. & Maldarelli, C. 1998 Theory and experiment on the low-Reynolds-number expansion and contraction of a bubble pinned at a submerged tube tip. *J. Fluid Mech.* **356**, 93–124.

Zhang, D. F. & Stone, H. A. 1997 Drop formation in viscous flows at a vertical capillary tube. *Phys. Fluids* **9**, 2234–2242.

Zhang, L. & Shoji, M. 2001 Aperiodic bubble formation from a submerged orifice. *Chem. Engng Sci.* **56**, 5371–5381.